The Equivalent Circuit of a Microstrip Crossover in a Dielectric Substrate

STILIANOS PAPATHEODOROU, STUDENT MEMBER, IEEE, ROGER F. HARRINGTON, FELLOW, IEEE, AND JOSEPH R. MAUTZ, SENIOR MEMBER, IEEE

Abstract—**A quasi-static analysis is carried out to examine the capacitive coupling between two nonintersecting orthogonal microstrip lines above a ground plane and in a dielectric substrate. The charge density along the width of each strip is described using a prescribed charge distribution. A pair of coupled integral equations is derived and solved via the method of moments to obtain the excess charge densities. The lumped excess capacitances are computed and compared to the ones obtained using wire lines with radii equal to the equivalent radii of the strips.**

I. Introduction and Statement of the Problem

MICROSTRIP structures in multilayered dielectric media have been analyzed extensively using a quasi-static approach provided that the strips are narrow compared to the wavelength. While for a homogeneous structure the dominant mode is TEM, when the structure is inhomogeneous the dominant mode becomes hybrid. However, at low frequencies the longitudinal field components are much smaller than the transverse components, justifying the quasi-static approximation.

In this paper we are seeking the equivalent circuit of two nonintersecting orthogonal narrow conducting strips of widths $2\alpha_1$ and $2\alpha_2$ and of infinite length above and parallel to a perfectly conducting plane. The top strip lies on the boundary between two different dielectric media. This boundary is a plane which is parallel to the perfectly conducting plane. Figs. 1 and 2 show the geometry of the structure and the equivalent lumped element circuit. This inhomogeneous structure, which we will refer to as a microstrip crossover, is widely used in microwave and millimeter-wave integrated circuits and microelectronic packaging.

As in [1] and [2], the present paper uses a Green's function for two layers of dielectric above a ground plane and a quasi-TEM analysis. In [3] the homogeneous crossover between two ground planes is analyzed using an iterative algorithm, while in [4] the crossover is enclosed between ground planes and conducting walls, and a transverse resonance analysis is carried out. In [5] a full-wave analysis is carried out for a semi-infinite crossover. The Green's function which is used in our problem is given in the form of a rapidly convergent infinite series and can be obtained as a three-dimensional (3-D) extension of the results given in [6]–[8]. To relate the excess charges to the stripline potentials a pair of coupled integral equations is obtained, which are solved via the method of moments with point matching [9]. The number of unknowns is reduced significantly by introducing a transverse charge distribution that satisfies the edge condition [10]. This distribution introduces integrals that can be evaluated efficiently using a numerical algorithm called Gauss–Chebyshev quadrature.

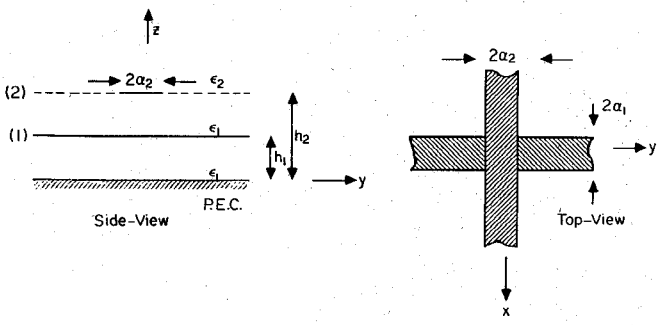

Fig. 1. Geometry of the microstrip structure.

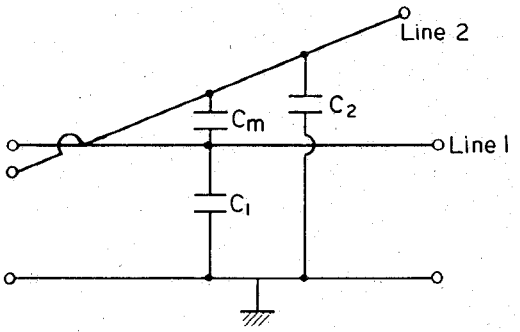

Fig. 2. Equivalent circuit of the microstrip crossover consisting of lumped excess capacitances.

Manuscript received November 7, 1988; revised August 3, 1989. This work was supported by the New York State Center for Advanced Technology in Computer Applications and Software Engineering (CASE), Syracuse University, Syracuse, NY 13244, and by the U.S. Army Research Office, Research Triangle Park, NC 27709, under Contract DAAL03-88-K-0133.

The authors are with the Department of Electrical and Computer Engineering, Syracuse University, Syracuse, NY 13244-1240.

IEEE Log Number 8932868.

0018-9480/90/0200-0135$01.00 ©1990 IEEE

II. Analysis

The position-dependent charges per unit area on striplines 1 and 2 are defined as in [11] by

$$Q_1(x, y) = Q_{10}(x) + q_1(x, y) \tag{1}$$

for line 1 and

$$Q_2(x, y) = Q_{20}(y) + q_2(x, y) \tag{2}$$

for line 2. If ϕ_1 is the potential on line 1 then Q_{10} is the charge per unit area required to maintain ϕ_1 in the absence of the other line. Charge density Q_{20} is defined in a similar manner for line 2. Because the densities q_1 and q_2 exist in excess of Q_{10} and Q_{20}, they are called excess charge densities. The potential at a point R in the ϵ_i medium above the ground plane is due to the total charge densities on lines 1 and 2 and is given by

$$\phi(\boldsymbol{R}) = \sum_{j=1}^{2} \int\int_{S_j} Q_j(R') G_{ij}(\boldsymbol{R}|\boldsymbol{R}')\, ds'$$

or, in a symbolic notation,

$$\phi(\boldsymbol{R}) = \phi(Q_1, G_{i1}) + \phi(Q_2, G_{i2}), \qquad i = 1,2. \tag{3}$$

Here, S_j is the surface of strip j, Q_j is the charge density on it, and $G_{ij}(\boldsymbol{R}|\boldsymbol{R}')$ with $(i, j = 1,2)$ is the electrostatic 3-D Green's function given in Appendix I.

From the definition of Q_{10} and Q_{20} we have that

$$\phi_i = \phi(Q_{i0}, G_{i1}), \qquad i = 1,2. \tag{4}$$

Note that when $R, R' \in S_2$ then $G_{22} = G_{21}$. Introducing (1), (2), and (4) into (3) and specializing the resulting equations to striplines 1 and 2, we obtain the pair of coupled integral equations

$$\phi(q_1, G_{11}) + \phi(q_2, G_{12}) = -\phi(Q_{20}, G_{12}) \tag{5}$$

and

$$\phi(q_1, G_{21}) + \phi(q_2, G_{21}) = -\phi(Q_{10}, G_{21}). \tag{6}$$

We next let

$$Q_{i0} = \phi_i \hat{Q}_{i0}, \qquad i = 1,2 \tag{7}$$

which when used in (4), (5), and (6) gives

$$1 = \phi(\hat{Q}_{10}, G_{11}) \tag{8}$$

$$1 = \phi(\hat{Q}_{20}, G_{21}) \tag{9}$$

$$\phi(\hat{q}_{11}, G_{11}) + \phi(\hat{q}_{21}, G_{12}) = 0 \tag{10a}$$

$$\phi(\hat{q}_{11}, G_{21}) + \phi(\hat{q}_{21}, G_{21}) = -\phi(\hat{Q}_{10}, G_{21}) \tag{10b}$$

and

$$\phi(\hat{q}_{12}, G_{11}) + \phi(\hat{q}_{22}, G_{12}) = -\phi(\hat{Q}_{20}, G_{12}) \tag{11a}$$

$$\phi(\hat{q}_{12}, G_{21}) + \phi(\hat{q}_{22}, G_{21}) = 0. \tag{11b}$$

The new quantities $\hat{q}_{ij}$ are related to q_1 and q_2 via

$$q_1 = \phi_1 \hat{q}_{11} + \phi_2 \hat{q}_{12} \tag{12}$$

$$q_2 = \phi_1 \hat{q}_{21} + \phi_2 \hat{q}_{22}. \tag{13}$$

The net excess charges Q_1^e and Q_2^e of lines 1 and 2 are obtained by integrating q_1 and q_2 over the corresponding line. These net charges are then related to the line potentials through the coefficients of capacitance and induction C_{ii} and C_{ij} respectively [12]. Then we have

$$Q_1^e = c_{11}\phi_1 + c_{12}\phi_2 \tag{14}$$

$$Q_2^e = c_{21}\phi_1 + c_{22}\phi_2. \tag{15}$$

Next the lumped excess capacitances are given by

$$C_1 = c_{11} + c_{12} \tag{16}$$

$$C_2 = c_{21} + c_{22} \tag{17}$$

$$C_m = -c_{12}. \tag{18}$$

C_1 and C_2 are the excess capacitances of lines 1 and 2 respectively and C_m is their mutual capacitance. The coefficients of capacitance and induction are related to the excess densities through

$$c_{1j} = \int_{-\alpha_1}^{\alpha_1} dx \int_{-\infty}^{\infty} dy\, \hat{q}_{1j}(x, y) \tag{19}$$

and

$$c_{2j} = \int_{-\alpha_2}^{\alpha_2} dy \int_{-\infty}^{\infty} dx\, \hat{q}_{2j}(x, y), \qquad j = 1,2. \tag{20}$$

III. Moment Solution

Our objective now is to solve (8) and (9) for $\hat{Q}_{10}$ and $\hat{Q}_{20}$ respectively and then to use these quantities in (10a), (10b) and (11a), (11b). To this end we let the unperturbed stripline density $\hat{Q}_{10}(x)$ be approximated by

$$\hat{Q}_{10}(x) = \frac{A_1}{\sqrt{\alpha_1^2 - x^2}} \tag{21}$$

where A_1 is an unknown constant. To represent $\hat{Q}_{20}(y)$ we replace A_1, α_1, and x with A_2, α_2, and y respectively in (21) above. Introducing (21) and (A1) into (8) and performing the integration with respect to y, the integral with respect to x is evaluated numerically, as shown in [13], using the Gauss–Chebyshev quadrature [14]. Special care should be exercised due to singularities of the logarithmic kernel. We then compute A_1 and, in a similar manner, A_2.

We next approximate the excess densities as

$$\hat{q}_{1j} = \frac{1}{\sqrt{\alpha_1^2 - x^2}} \sum_{n=1}^{N} \hat{q}_{1j,n} P_n(y) \tag{22}$$

for line 1 and

$$\hat{q}_{2j} = \frac{1}{\sqrt{\alpha_2^2 - y^2}} \sum_{n=1}^{N} \hat{q}_{2j,n} P_n(x), \qquad j = 1,2 \tag{23}$$

for line 2. Here, $P_n(x)$ is the pulse function defined by

$$P_n(x) = \begin{cases} 1, & -L + (n-1)\Delta \leqslant x < -L + n\Delta \\ 0, & \text{otherwise} \end{cases} \tag{24}$$

where L is an appropriately chosen length and

$$\Delta = \frac{2L}{N}. \tag{25}$$

Next we introduce (21), (22), and (23) into (10a), (10b) and (11a), (11b) and satisfy the resulting equations at the

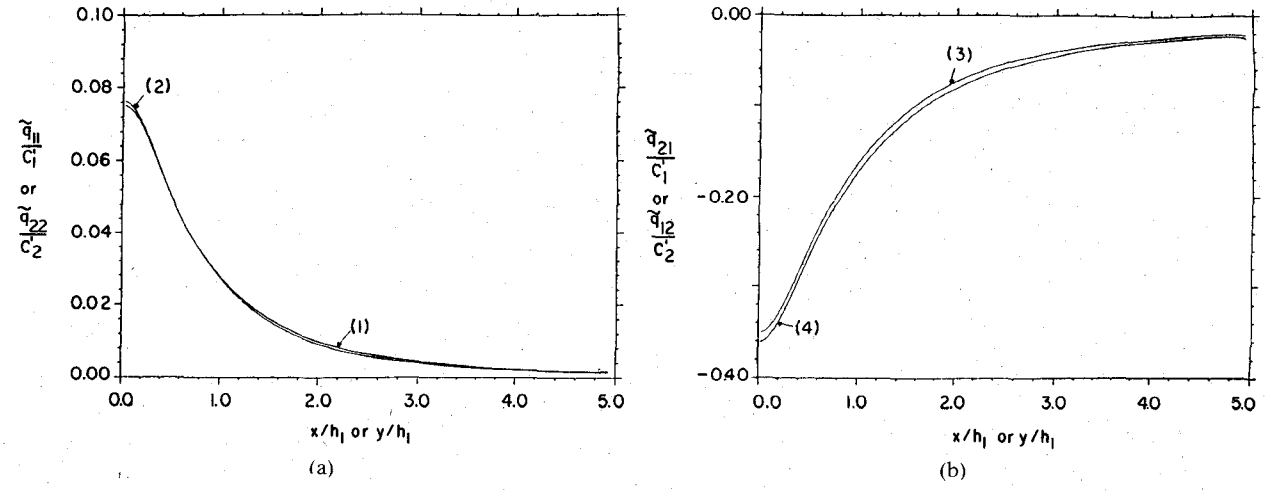

Fig. 3. Normalized excess charge densities when $\alpha_1 = \alpha_2 = 0.02h_1$, $h_2/h_1 = 1.5$, $\epsilon_1 = \epsilon_2 = \epsilon_0$. (1) $\tilde{q}_{11}/C_1'$ versus y/h_1; (2) $\tilde{q}_{22}/C_2'$ versus x/h_1; (3) $\tilde{q}_{21}/C_1'$ versus x/h_1; (4) $\tilde{q}_{12}/C_2'$ versus y/h_1.

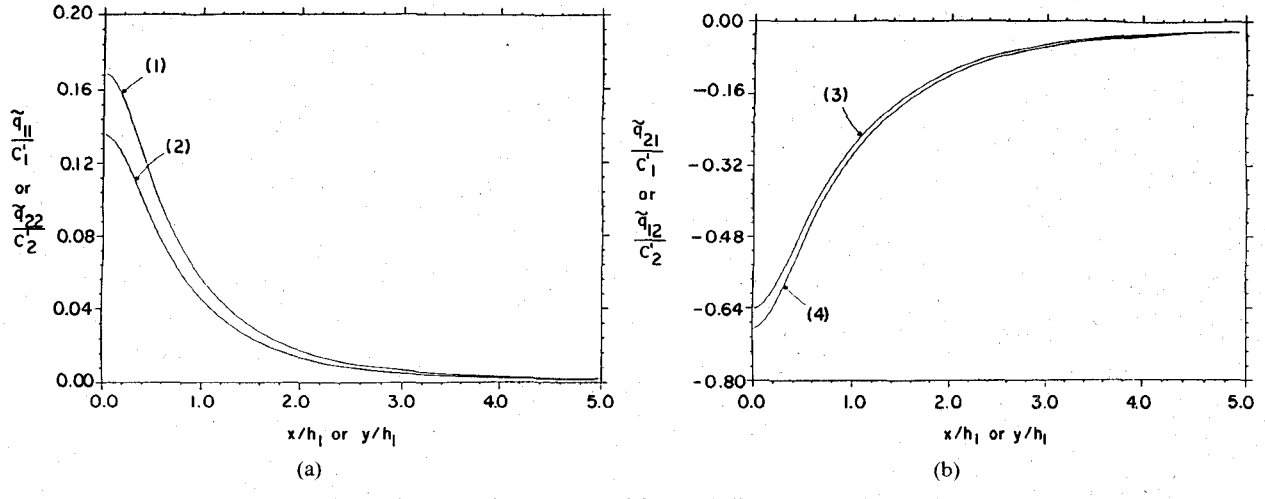

Fig. 4. Normalized excess charge densities when $\alpha_1 = \alpha_2 = 0.02h_1$, $h_2/h_1 = 1.5$, $\epsilon_1 = 2\epsilon_0$, and $\epsilon_2 = \epsilon_0$. (1) $\tilde{q}_{11}/C_1'$ versus y/h_1; (2) $\tilde{q}_{22}/C_2'$ versus x/h_1; (3) $\tilde{q}_{21}/C_1'$ versus x/h_1; (4) $\tilde{q}_{12}/C_2'$ versus y/h_1.

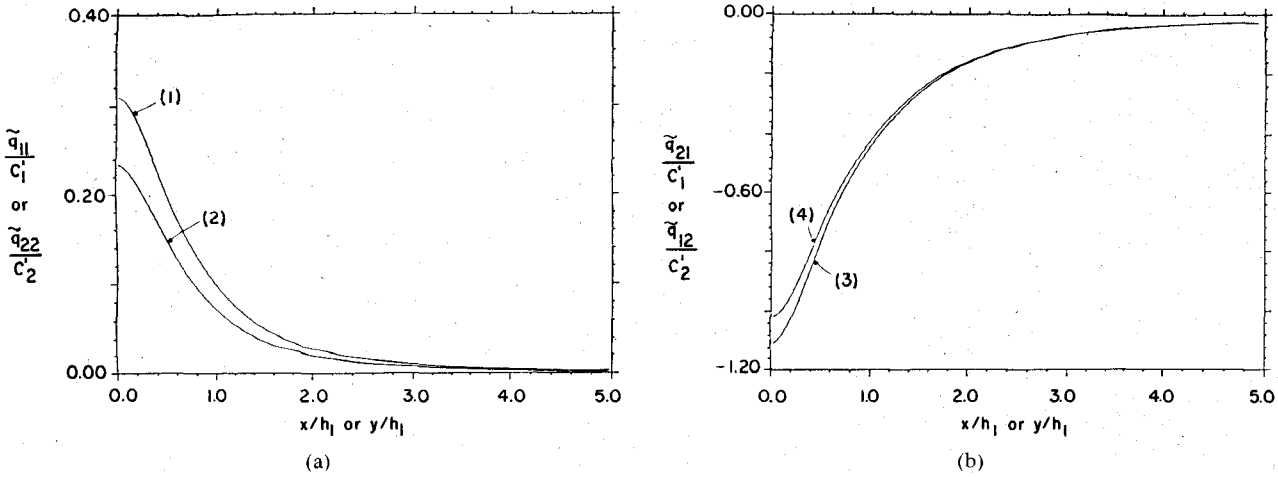

Fig. 5. Normalized excess charge densities when $\alpha_1 = 0.02h_1$, $\alpha_2 = 0.04h_1$, $\epsilon_1 = 3\epsilon_0$, and $\epsilon_2 = \epsilon_0$. (1) $\tilde{q}_{11}/C_1'$ versus y/h_1; (2) $\tilde{q}_{22}/C_2'$ versus x/h_1; (3) $\tilde{q}_{21}/C_1'$ versus x/h_1; (4) $\tilde{q}_{12}/C_2'$ versus y/h_1.

midpoint of the domain of each function along the axis of each strip. The matrix equations obtained are of the form

$$[K]\begin{bmatrix}\vec{q}_{11}\\ \vec{q}_{21}\end{bmatrix}=\begin{bmatrix}0\\ -A_1\vec{l}\end{bmatrix} \tag{26}$$

and

$$[K]\begin{bmatrix}\vec{q}_{12}\\ \vec{q}_{22}\end{bmatrix}=\begin{bmatrix}-A_2\vec{g}\\ 0\end{bmatrix}. \tag{27}$$

The form of the system matrix K and the source vectors $\vec{l}$ and $\vec{g}$ are shown in Appendix II. From (22), (23), (19), and (20) we also obtain

$$c_{1j}=\pi\Delta\sum_{n=1}^{N}\hat{q}_{1j,n} \tag{28}$$

and

$$c_{2j}=\pi\Delta\sum_{n=1}^{N}\hat{q}_{2j,n},\qquad j=1,2. \tag{29}$$

IV. Numerical Results

Figs. 3–5 show the plots of the excess charge densities versus the normalized distance from the center of symmetry. The quantities that we have plotted are $\tilde{q}_{1i}(y)/C_i'$, where

$$\tilde{q}_{1i}(y)=\int_{-\alpha_1}^{\alpha_1}\hat{q}_{1i}(x,y)\,dx$$

for strip 1 and $\tilde{q}_{2i}(x)/C_i'$, where

$$\tilde{q}_{2i}(x)=\int_{-\alpha_2}^{\alpha_2}\hat{q}_{2i}(x,y)\,dy$$

for strip 2, with $i=1, 2$. C_1' and C_2' are the capacitances per unit length of the isolated wire lines with radii equal to the equivalent radii of striplines 1 and 2 respectively. C_1' and C_2' are calculated with $\epsilon_1=\epsilon_2=\epsilon_0$, where ϵ_0 is the permittivity of free space. As is shown in [15], the equivalent radius of a narrow strip is equal to one fourth its width. It has been found that the excess charge density is concentrated within a length of about $20h_2$ or $30h_2$, outside of which it is negligible. However, when computing we assumed a length $10h_1$ for each strip. Otherwise stated, $L=5h_1$ in (24) and (25). The height ratio h_2/h_1 was taken equal to 1.5 and the length of each subsection $5\times10^{-2}h_1$. In Fig. 3 the permittivities ϵ_1 and ϵ_2 were chosen to be equal to ϵ_0, and the widths of both strips $4\times10^{-2}h_1$ or $\alpha_1=\alpha_2=0.02h_1$. These plots then were compared to the ones shown in [11], [16], and [17], where the same parameters were used, and the agreement was excellent. In particular the plots of Fig. 3 are identical to the ones of [17], as expected. When the dielectric interface ceases to exist the infinite series that represents the 3-D Green's function reduces to that of free space, which is the case treated in [17]. In [16] the wire and strip crossovers are examined in free space. The width of each strip was divided into N' subsections. To compare the wire and the strip crossover we assumed a wire with radius equal to the strip's equivalent radius. Table I shows the values of the normalized

TABLE I
Comparison of Results for Fig. 3

	Results obtained using [16] (wire crossover)	Results obtained using [16] for a strip crossover with N' pulses along its width		Results obtained using [17]	Present solution
		N'=12	N'=6		
$\frac{C_m}{h_1C_2'}$	1.013	1.002	0.991	1.014	1.014
$\frac{C_1}{h_1C_1'}$	-0.853	-0.844	-0.836	-0.853	-0.853
$\frac{C_2}{h_1C_2'}$	-0.792	-0.785	-0.777	-0.792	-0.792

TABLE II
Results for Figs. 4 and 5

	$\alpha_1=\alpha_2=0.02\,h_1$ $\epsilon_1=2\epsilon_0$, $\epsilon_2=\epsilon_0$	$\alpha_1=0.02\,h_1$, $\alpha_2=0.04\,h_1$ $\epsilon_1=3\epsilon_0$, $\epsilon_2=\epsilon_0$
$\frac{C_m}{h_1C_2'}$	1.672	2.337
$\frac{C_1}{h_1C_1'}$	-1.345	-1.763
$\frac{C_2}{h_1C_2'}$	-1.296	-2.056

lumped excess capacitances using [16]. As expected by increasing the number of subsections N', the agreement between the two solutions becomes excellent, as is the agreement with the solution presented in [11]. However, increasing N' results in an excessive computation time. To reduce the computation time we then introduced the transverse charge distributions (21)–(23). These distributions satisfy the edge conditions [10]. The results obtained and shown in [17] were again in excellent agreement with the previous ones, as is shown in Table I. Due to a substantial decrease in the number of unknowns, the computation time was greatly reduced.

In Fig. 4 we have chosen $\epsilon_1=2\epsilon_0$ and $\epsilon_2=\epsilon_0$. The infinite series that represents the 3-D Green's function is fast converging, and ten terms ($M=10$) gave excellent accuracy. As a final example Fig. 5 shows the normalized densities when $\alpha_1=0.02h_1$, $\alpha_2=0.04h_1$, $\epsilon_1=3\epsilon_0$, and $\epsilon_2=\epsilon_0$. The normalized excess capacitances that correspond to Figs. 4 and 5 are shown in Table II.

V. Conclusion

The capacitive coupling between two nonintersecting orthogonal microstrip lines inside a dielectric medium (μ_0, ϵ_1) interfacing an infinite dielectric layer (μ_0, ϵ_2) was examined. The analysis was carried out using the electrostatic 3-D Green's function and the method of moments. An edge condition was assumed to describe the excess charge distribution along the widths. This approach simplifies the analysis and drastically reduces the computation time. The results obtained for the limiting case $\epsilon_1=\epsilon_2$ were compared with results obtained using a solution

where the width distribution was treated as unknown and determined by the moment solution. The agreement between the two approaches was excellent.

APPENDIX I

The electrostatic three-dimensional Green's function for a two-layer dielectric above a perfectly conducting plane consists of four expressions depending on the location of the field and source points. Thus, as is shown in [13],

$$G(\boldsymbol{R}|\boldsymbol{R}') = \begin{cases} G_{11}(\boldsymbol{R}|\boldsymbol{R}'), & z \leqslant h_2, z' \leqslant h_2 \\ G_{12}(\boldsymbol{R}|\boldsymbol{R}'), & z \leqslant h_2, z' \geqslant h_2 \\ G_{22}(\boldsymbol{R}|\boldsymbol{R}'), & z \geqslant h_2, z' \geqslant h_2 \\ G_{21}(\boldsymbol{R}|\boldsymbol{R}'), & z \geqslant h_2, z' \leqslant h_2. \end{cases}$$

Here

$$G_{11} = \frac{1}{4\pi\epsilon_1}\left[\sum_{i=0}^{\infty}(-1)^i E^i \cdot\left(\frac{1}{\sqrt{(x-x')^2+(y-y')^2+(z-z'+2ih_2)^2}} - \frac{1}{\sqrt{(x-x')^2+(y-y')^2+(z+z'+2ih_2)^2}}\right) - \sum_{i=0}^{\infty}(-1)^{i+1}E^{i+1} \cdot\left(\frac{1}{\sqrt{(x-x')^2+(y-y')^2+(z+z'-2(i+1)h_2)^2}} - \frac{1}{\sqrt{(x-x')^2+(y-y')^2+(z-z'-2(i+1)h_2)^2}}\right)\right] \tag{A1}$$

$$G_{12} = \frac{1}{2\pi(\epsilon_1+\epsilon_2)}\sum_{i=0}^{\infty}(-1)^i E^i \cdot\left(\frac{1}{\sqrt{(x-x')^2+(y-y')^2+(z-z'-2ih_2)^2}} - \frac{1}{\sqrt{(x-x')^2+(y-y')^2+(z+z'+2ih_2)^2}}\right) \tag{A2}$$

$$G_{22} = \frac{1}{4\pi\epsilon_2}\left[\frac{1}{\sqrt{(x-x')^2+(y-y')^2+(z-z')^2}} - \frac{E}{\sqrt{(x-x')^2+(y-y')^2+(z+z'-2h_2)^2}} - \sum_{i=0}^{\infty}\frac{(-1)^i E^i(1-E^2)}{\sqrt{(x-x')^2+(y-y')^2+(z+z'+2ih_2)^2}}\right] \tag{A3}$$

and

$$G_{21} = \frac{1}{2\pi(\epsilon_1+\epsilon_2)}\sum_{i=0}^{\infty}(-1)^i E^i \cdot\left(\frac{1}{\sqrt{(x-x')^2+(y-y')^2+(z-z'+2ih_2)^2}} - \frac{1}{\sqrt{(x-x')^2+(y-y')^2+(z+z'+2ih_2)^2}}\right). \tag{A4}$$

Note that

$$E = \frac{\epsilon_1-\epsilon_2}{\epsilon_1+\epsilon_2}.$$

Both G_{11} and G_{12} vanish at $z=0$, as expected. It can also be shown that the tangential electric field and normal electric displacement are continuous across the dielectric interface. At $z'=h_2$, we have $G_{12}=G_{11}$ and $G_{21}=G_{22}$.

APPENDIX II

A. The System Matrix K

The system matrix K consists of four submatrices and is of the form

$$[K] = \begin{bmatrix} [k^{11}] & [k^{12}] \\ [k^{21}] & [k^{22}] \end{bmatrix} \tag{A5}$$

where the elements of submatrices k^{11}, k^{12}, k^{21}, and k^{22} are

$$k_{mn}^{11} = \int_{-\alpha_1}^{\alpha_1}\frac{dx'}{\sqrt{\alpha_1^2-x'^2}}\int_{y_n}^{y_{n+1}} dy' G_{11}(0, y_m^+, h_1|x', y', h_1) \tag{A6}$$

$$k_{mn}^{12} = \int_{-\alpha_2}^{\alpha_2}\frac{dy'}{\sqrt{\alpha_2^2-y'^2}}\int_{\hat{x}_n}^{\hat{x}_{n+1}} dx' G_{12}(0, y_m^+, h_1|x', y', h_2) \tag{A7}$$

$$k_{mn}^{21} = \int_{-\alpha_1}^{\alpha_1}\frac{dx'}{\sqrt{\alpha_1^2-x'^2}}\int_{y_n}^{y_{n+1}} dy' G_{21}(\hat{x}_m^+, 0, h_2|x', y', h_1) \tag{A8}$$

and

$$k_{mn}^{22} = \int_{-\alpha_2}^{\alpha_2}\frac{dy'}{\sqrt{\alpha_2^2-y'^2}}\int_{\hat{x}_n}^{\hat{x}_{n+1}} dx' G_{21}(\hat{x}_m^+, 0, h_2|x', y', h_2). \tag{A9}$$

Here (y_n, y_{n+1}) is the domain of $P_n(y)$ along the length of strip 1, and $(\hat{x}_n, \hat{x}_{n+1})$ is the domain of $P_n(x)$ along the length of strip 2. Furthermore, $y_m^+ = (y_m + y_{m+1})/2$ and $\hat{x}_m^+ = (\hat{x}_m + \hat{x}_{m+1})/2$. In the expressions above we perform a straightforward integration of the Green's function over the domain of each pulse. The integration along the width of each strip is performed numerically using the Gauss–

Chebyshev quadrature. However, caution should be exercised with expressions (A6) and (A9) due to occurring singularities.

B. The Source Vectors $\vec{l}, \vec{y}$

Introducing (21) into (10b) we find the source vector $\vec{l}$ whose mth element is

$$l_m = \int_{-\alpha_1}^{\alpha_1} \frac{dx'}{\sqrt{\alpha_1^2 - x'^2}} \int_{-\infty}^{\infty} dy' G_{21}(\hat{x}_m^+, 0, h_2 | x', y', h_1). \tag{A10}$$

Similarly, we obtain

$$g_m = \int_{-\alpha_2}^{\alpha_2} \frac{dy'}{\sqrt{\alpha_2^2 - y'^2}} \int_{-\infty}^{\infty} dx' G_{12}(0, y_m^+, h_1 | x', y', h_2). \tag{A11}$$

The double integrals in (A10) and (A11) are evaluated in the same manner as those in (A6)–(A9).

References

[1] C. Wei and R. F. Harrington, "Computation of the parameters of multiconductor transmission lines in two dielectric layers above a ground plane," Department of Electrical and Computer Engineering, Syracuse University, Rep. TR-82-12, Nov. 1982.

[2] W. T. Weeks, "Calculation of coefficients of capacitance of multiconductor transmission lines in the presence of a dielectric interface," *IEEE Trans. Microwave Theory Tech.*, vol. MTT-18, pp. 35–43, Jan. 1970.

[3] C. H. Chan and R. Mittra, "Analysis of MMIC structures using an efficient iterative approach," *IEEE Trans. Microwave Theory Tech.*, vol. 36, pp. 96–105, Jan. 1988.

[4] T. Uwano, R. Sorrentino, and T. Itoh, "Characterization of strip line crossing by transverse resonance analysis," *IEEE Trans. Microwave Theory Tech.*, vol. MTT-35, pp. 1369–1376, Dec. 1987.

[5] H. -Y. Yang and N. G. Alexopoulos, "Basic blocks for high-frequency interconnects: Theory and experiment," *IEEE Trans. Microwave Theory Tech.*, vol. 36, pp. 1258–1264, Aug. 1988.

[6] P. Silvester, "TEM wave properties of microstrip transmission lines," *Proc. Inst. Elec. Eng.*, vol. 115, pp. 43–48, Jan. 1968.

[7] R. Crampagne and J. -L. Guiraud, "A two- or three-dimensional Green's function which can be applied to hyperfrequency microelectronic transmission lines," *IEEE Trans. Microwave Theory Tech.*, vol. MTT-25, pp. 442–444, May 1977.

[8] S. Coen, "A note on Green's function for microstrip," *IEEE Trans. Microwave Theory Tech.*, vol. MTT-23, pp. 591–593, July 1975.

[9] R. F. Harrington, *Field Computation by Moment Methods*. New York: Macmillan, 1968. Reprinted by Krieger Publishing, Melbourne, FL, 1982.

[10] C. M. Butler and D. R. Wilton, "General analysis of narrow strips and slots," *IEEE Trans. Antennas Propagat.*, vol. AP-28, pp. 42–48, Jan. 1980.

[11] D. V. Giri, S.-K. Chang, and F. M. Tesche, "A coupling model for a pair of skewed transmission lines," *IEEE Trans. Electromagn. Compat.*, vol. EMC-22, pp. 20–28, Feb. 1980.

[12] R. Plonsey and R. E. Collin, *Principles and Applications of Electromagnetic Fields*. New York: McGraw-Hill, 1961.

[13] S. Papatheodorou, J. R. Mautz, and R. F. Harrington, "The equivalent circuit of a microstrip crossover in a dielectric substrate," Department of Electrical and Computer Engineering, Syracuse University, Syracuse, NY, Rep. TR-88-11, Aug. 1988.

[14] B. Carnahan, H. A. Luther, and J. O. Wilkes, *Applied Numerical Methods*. New York: Wiley, 1969.

[15] C. Butler, "The equivalent radius of a narrow conducting strip," *IEEE Trans. Antennas Propagat.*, vol. AP-30, pp. 755–758, July 1982.

[16] S. Papatheodorou, R. F. Harrington, and J. R. Mautz, "The equivalent circuit of two non-intersecting strip lines parallel to a conducting plane and perpendicular to each other," Department of Electrical and Computer Engineering, Syracuse University, Syracuse, NY, Rep. TR-88-3, Apr. 1988.

[17] S. Papatheodorou, R. F. Harrington, and J. R. Mautz, "A quasi-static analysis of a microstrip crossover using a prescribed transverse charge distribution," Department of Electrical and Computer Engineering, Syracuse University, Syracuse, NY, Rep. TR-88-4, July 1988.

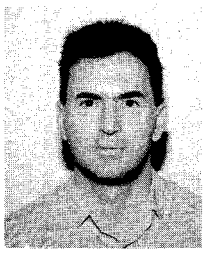

Stilianos Papatheodorou (S' 82) received the B.S. degree (magna cum laude) from Syracuse University, Syracuse, NY, in 1981 and the M.S. degree from the Ohio State University in 1983, both in electrical engineering. He received the Ph.D. degree from Syracuse University in December 1989. His research interests include field analysis of printed circuits, numerical methods in electromagnetics, and signal processing.

Dr. Papatheodorou is a member of Tau Beta Pi.

Roger F. Harrington (S'48–A'53–M'57–SM'62–F'68) was born in Buffalo, NY, on December 24, 1925. He received the B.E.E. and M.E.E. degrees from Syracuse University, Syracuse, NY, in 1948 and 1950, respectively, and the Ph.D. degree from Ohio State University, Columbus, in 1952.

From 1945 to 1946, he served as an Instructor at the U.S. Naval Radio Materiel School, Dearborn, MI, and from 1948 to 1950 he was employed as an Instructor and Research Assistant at Syracuse University. While studying at Ohio State University, he served as a Research Fellow in the Antenna Laboratory. Since 1952, he has been on the faculty of Syracuse University, where he is presently Professor of Electrical Engineering. During the years 1959–1960, he was visiting Associate Professor at the University of Illinois, Urbana; in 1964 he was Visiting Professor at the University of California, Berkeley; and in 1969 he was Guest Professor at the Technical University of Denmark, Lyngby, Denmark.

Dr. Harrington is a member of Tau Beta Pi, Sigma Xi, and the American Association of University Professors.

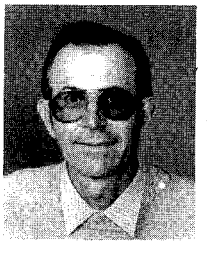

Joseph R. Mautz (S'66–M'67–SM'75) was born in Syracuse, NY, on April 29, 1939. He received the B.S., M.S., and Ph.D. degrees in electrical engineering from Syracuse University, Syracuse, NY, in 1961, 1965, and 1969, respectively.

He is a Research Engineer in the Department of Electrical Engineering, Syracuse University, working on radiation and scattering problems. His primary fields of interest are electromagnetic theory and applied mathematics. He is currently working in the area of numerical methods for solving field problems.